Effects of Nonuniform Corrosion on the Structural Failure of Galvanized Steel Lattice Transmission Towers in Hurricanes

A Thesis

Presented to

Faculty of the Department of Civil, Environmental and Geodetic Engineering

The Ohio State University

In Partial Fulfillment

of the Requirements for

Honors Research Distinction

by

Keoni Sanny

April, 2020

ABSTRACT

This study establishes a framework for evaluating the structural performance of steel lattice transmission towers experiencing the effects of realistic, nonuniform corrosion. It is shown that different patterns of geometry, size, orientation, and elevation-dependent nonuniform corrosion change structural performance as compared to the traditional assumption of uniform corrosion over the whole tower. Additionally, modelling the variable zinc coating thickness observed in actual galvanized steel towers is observed to affect performance as compared to previous studies that used a constant protective coating thickness. Further research is needed to fully understand the nature of these effects on tower performance.

ACKNOWLEDGEMENTS

The author would like to express his deep gratitude to Dr. Abdollah Shafieezadeh, his research advisor, and Dr. Jieun Hur for their guidance and support. They undoubtedly opened doors for the author's future and made this study possible.

The author is also thankful for being able to work with and learn from Yousef Mohammadi Darestani and Ashkan Bagheri Jeddi. This study could not have been completed without their help.

Finally, the author would like to thank his family and friends for their support. He could not have made it this far without them.

TABLE OF CONTENTS

Page

CHAPTER 1

1INTRODUCTION

1.1. MOTIVATION

Galvanized steel lattice towers are the most common supporting structure for carrying overhead conductors in power transmission networks in the United States. These towers are subject to failure when exposed to high wind speeds such as those experienced during hurricanes, especially when corrosion has weakened tower components. State-of-the-art research has characterized tower failure modes with wind testing simulations in sophisticated FE models, but these studies have largely been performed on as-new (zero corrosion) structures. For those studies that have modeled tower failure after corrosion has occurred, the corrosion attack has been simplified as a uniform loss of thickness over the entire tower. In reality, corrosion rates can vary widely depending on a metal object's size, shape, elevation, rain exposure, and exposure to wind from particular directions. Additionally, zinc coating thickness for galvanized towers has been assumed to be constant over the entire structure, when in reality coating thickness from the hot-dip process is highly dependent on the size of the member.

Widespread and long-lasting storm-related power outages have strained communities around the country every year and incurred $20 to $55 billion of annual loss to the US economy (Campbell, 2012). As power transmission infrastructure carries bulk power over long distances, its failure of during storms is a critical part of the problem. In 2016, for example, Hurricane Matthew destroyed 58 transmission towers on its way to causing 1.4 million people to lose power (Downey, 2018). Transmission tower failure is a critical issue for the economy and public safety, and thus the true behavior of corroded transmission towers under extreme loading should be known in order to adequately design and maintain these structures.

1.2. OBJECTIVES

This research sets out to establish a framework for evaluating the structural performance of steel lattice transmission towers experiencing the effects of realistic, nonuniform corrosion. The hurricane simulation performance of galvanized steel towers experiencing nonuniform corrosion will then be compared to towers experiencing uniform attack – the traditional assumption. This study also aims to compare the effects of different corrosion patterns and protective zinc coating thickness distributions on tower performance.

CHAPTER 2

LITERATURE SURVEY

2.1. INTRODUCTION

A survey of the literature is presented in this chapter regarding corroding transmission tower failure analysis, prediction of geometry-based corrosion attack, and field observations of corrosion patterns.

2.2. COMPUTATIONAL ANALYSIS OF CORRODED TRANSMISSION TOWERS

To the author's knowledge, only three studies in the literature have modeled the structural capacity of corroded galvanized steel transmission towers. Salazar and Mendoza (2008) studied a 40 m tall, galvanized steel, 400 kV-carrying tower using FEM analysis. The model allows tower members to bend and considers bolt slippage and deformation. 14 design load cases – used for the original design of the actual tower – are applied to the tower using FEM as a uniform, deterministic corrosion rate is applied to all components excepting connections. A uniform coating thickness of 85 μm on all tower surfaces is assumed. Static and modal analysis were thus carried out. In the modal analysis, natural frequencies of the tower for each load case were calculated, and it was found that vibration damage would not be likely to cause tower failure for the considered conditions. For static analysis, however, tower failure is predicted to occur when a thickness loss of 3 mm on all members has occurred, while 2.5 mm thickness loss was found to be safe. The 2.5 mm and 3 mm cases were calculated to occur after 118 and 140 years of service life, respectively.

Niu et al. (2017) conducted actual wind tunnel tests using a 1/40 scale model tower to obtain the tower and cable drag coefficients for FEM analysis. Instead of just transverse and longitudinal loading, 0°, 30°, 60°, and 90° wind attack was studied. For modeling of corrosion, the structure is assumed to be painted; a constant initiation time is thus assumed (5 years) before deterioration of

the steel substrate begins, at which point a uniform, deterministic corrosion rate is applied on all components except connections. ANSYS is used to model three 68.6 m tall transmission towers connected by conductors. Geometric and material nonlinearity are both considered, but, like Salazar and Mendoza (2008), joint failure and uncertainty of construction material properties are not considered. Incremental dynamic analysis was then conducted using wind time histories. It was found that corrosion decreased the capacity of the system and increased tower top displacement, particularly for transverse wind attack. In addition, for the corroded model, consideration of the aerodynamic damping force of the conductors increased the capacity of the system in comparison to simulations without the aerodynamic damping force. The aerodynamic damping force had little effect on the non-corroded model, however.

Cha (2019) used a sophisticated finite element model to assess the effect of corrosion on a transmission tower made of weathering steel. Material uncertainty, wind loading uncertainty, connection failures, and uncertain corrosion rate on members and connections were all considered. The effects of structural member orientation, size, and elevation on corrosion rate were neglected, however. Corrosion in a simulated moderate marine environment was found to decrease the maximum load factor about 10% for transverse wind loading and 5% for longitudinal loading after 60 years.

2.3. PREDICTING GEOMETRY-DEPENDENT ATMOSPHERIC CORROSION RATE

As corrosion in marine locations is driven in large part by the quantity of sea salt aerosol deposited on a surface, Klassen and Roberge (2000) sought to a method to model the deposition flux J_y of aerosol to objects of different size and shape. They proposed the following formulation:

$$J_y = -D^t \frac{\partial C}{\partial y} \quad (2.3\text{-}1)$$

where $\frac{\partial C}{\partial y}$ is the concentration gradient of particles perpendicular to the surface and D^t is turbulent diffusivity. The authors go on to explicitly define D^t, which is direction-dependent and therefore requires estimation of the horizontal and vertical wind flux. FLUENT commercial software was then used to model the concentration gradient and turbulent diffusivity around a 2 by 3 m shed; despite the low aerosol concentration at the rear, the greatest deposition rates were found at the middle of the back and top surfaces of the shed due to high D^t values at these locations.

Klassen and Roberge (2000) and Klassen et al. (2000) also model aerosol deposition using a formulation based on inertial impaction:

$$R_d = C_\infty U_\infty A_t \eta\left(D_p, U_\infty, D_t, \rho_a\right) \quad (2.3\text{-}2)$$

where C_∞ is the upstream aerosol concentration, U_∞ is wind velocity, A_t is the projected target area, η is the capture efficiency of the object, D_p is particle diameter, D_t is target size, and ρ_a is aerosol density. The inertial impaction mechanism described by Equation (2.3-2) was estimated to be significant for small objects (that do not cause great changes to the surrounding airflow) as compared to the turbulent diffusivity described by Equation (2.3-1); particles strike the surface of small objects due to inertia instead of following disturbed flow lines around the object. Formulas for η have been estimated for simple shapes such as spheres and cylinders by assuming a fluid velocity profile around the object and have predicted greater capture efficiency with greater wind speed (Hidy, 1984). By substituting one of these formulas for a cylinder into Equation (2.3-2) in order to represent a salt candle, Klassen and Roberge (2000) and Klassen et al. (2000) calculated deposition rates by using FLUENT to model concentration and airflow (C_∞ and U_∞) at various points around the candle. Deposition near the base of the candle was found to be close to 0 due to

the low wind velocities there, whereas deposition was highest at the top of the candle due to high wind speed and aerosol concentration. Klassen et al. (2000) found good agreement with a field corrosivity study conducted in a tropical coastal environment in Australia. Corrosivity was found to increase with elevation at the site, and it was presumed that this was due to increasing wind speed, turbulence, and thus aerosol (chloride) deposition with height.

Cole and Paterson (2004) ran computational fluid dynamic (CFD) simulations on a supercomputer with the CFX4.3 CFD package in order to estimate the deposition rate of marine aerosols on objects. Deposition efficiency was found to increase with increasing turbulence intensity I:

$$\eta = 100 \cdot I \cdot C_s \qquad (2.3\text{-}3)$$

where the shape coefficient C_s is a constant dependent on the geometry of the target and I rises with increasing ground roughness and decreases with increasing elevation. In simulations of 150 by 95 mm plates, 95% of particles deposited on the front face, and C_s increased with decreasing angle from the horizontal: 0.5 for 90°, 1.2 for 45°, and 1.67 at 0° for fine particles of similar size as marine aerosol particles. Simulation for a salt candle – with a typical surface area on the order of 100 cm^2 (ISO 9225) compared to 1425 cm^2 per side for the simulated plates – revealed a lower deposition rate and a resulting C_s value of 0.85. Simulation on a 10 m high by 20 by 20 m building showed low deposition near the ground and on the rear and high deposition on the top and upper edges.

Compared with the other studies survey in this section, the model of Spence et al. (1992) is advantageous in that it (1) directly ties geometry and environmental factors (such as rainfall and SO_2 concentration) to corrosion rate and (2) it does not necessarily require CFD simulation to

obtain a solution. The model accounts for object geometry by including deposition velocity and horizontal angle terms directly in the formulation of zinc coating corrosion rate, $\frac{dC}{dt}$:

$$\begin{aligned}\frac{dC}{dt} &= a_0 R \cos(\theta_{Horiz})\, 10^{-pH}/t \\ &+ a_1 r R \cos(\theta) \exp(-21.34 + 3651/T)/t \\ &+ (0.045 V_d SO_2 t_w/t + SO_2 dry)\end{aligned} \tag{2.3-4}$$

where $\frac{dC}{dt}$ is in μm/year, a_0 and a_1 are size-dependent regression coefficients, r is a size-dependent rain residence time factor, R is total rainfall in cm during the exposure, θ_{Horiz} is the surface's angle from horizontal, pH is measured from rainfall, t is time in years, T is temperature in Kelvin, V_d is pollutant deposition velocity in cm/s, SO_2 is ambient concentration of SO_2 in μg/m^3, t_w is the time of wetness in years experienced by the surface, and $SO_2 dry$ is a climate-dependent constant – 0.035 μm/year for dry regions such as Denver, and 0.07 μm/year for other climate types.

Spence et al. (1992) derives V_d starting with the following expression:

$$V_d = V \cdot f(V, x) \tag{2.3-5}$$

where V is mean wind speed and x is some characteristic length – typically the distance the wind is in contact with the object. The form of function $f(V, x)$ is dependent on the turbulence of the boundary layer of airflow on an object's surface. Airflow is assumed to be laminar before it strikes an object; for small flat plates (on the order of 10 to 20 cm), airflow is thus assumed to remain laminar, and the familiar Blasius solution appears:

$$f(V, x)_{laminar} = \frac{1.328}{\sqrt{Re_x}} \cdot \frac{1}{2} = \frac{0.664}{\sqrt{Re_x}} \tag{2.3-6}$$

where Re_x is the Reynolds number calculated for the distance x that the airflow has been in contact with the plate:

$$Re_x = \frac{Vx}{\nu} \tag{2.3-7}$$

ν is the kinematic viscosity of air in cm^2/s. Similarly, for larger plates on the order of 70 cm long or greater, the airflow is assumed to become turbulent:

$$f(V,x)_{turbulent} = \frac{0.015}{{Re_x}^{1/7}} \tag{2.3-8}$$

When V_d is defined in cm/s, wind speed V in m/s, x in cm, and the kinematic viscosity of air in cm^2/s, substitution of Equations (2.3-8) and (2.3-7) into Equation (2.3-5) results in the expressions for small panels and larger sheets seen in Table 2.3-1 below. Table 2.3-1 also contains expressions for steel wire derived by Spence et al. (1992), along with the constants a_0, a_1, r.

Table 2.3-1. Model Coefficients for Different Galvanized Steel Structures (Spence et al., 1992)

Structure	a_0	a_1	r	V_d (cm/s)
10.2 by 15.2 cm panel	46	91.56	0.225	$6.64\sqrt{V\nu/x}$
10.2 by 20.4 cm panel	19.8	6.4	0.19	$6.64\sqrt{V\nu/x}$
71 by 91 cm sheet	39.7	23.8	0.3	$0.015(100V)^{6/7}(\nu/x)^{1/7}$
Wire (parallel)	14.6	13.1	0.3	$8\nu/x$
Wire (perpendicular)	14.6	13.1	0.3	$6.3\sqrt{V\nu/x}$

V is the mean annual wind speed (m/s)
ν is the kinematic viscosity of air (0.15 cm^2/s at 20°C)
x is the characteristic length of the structure (cm). For sheets and panels, x is always the length or width of member's face, never its thickness. x is diameter for wire.

The expressions for V_d derived in Table 2.3-1 reflect a specific set of assumptions about the deposition conditions. Firstly, it is assumed that the mean wind always carries pollutants to increase corrosion rate; in reality, wind from one direction at a site may carry pollutants, while wind from other directions may be relatively free and thus decrease corrosion rate. Secondly, it is assumed that for a given profile presented to the wind, deposition velocity decreases with an

increase in the size x of the object. This models the observations of Jeffrey and Melchers (2008) (described in section 2.4) and others of greater corrosion rate on smaller objects. A physical explanation of this phenomena is that bigger objects result in more airflow turbulence, preventing pollutants from settling onto the surface (Lipfert and Wyzga, 1986).

Referring back to Equation (2.3-4), Spence et al. (1992) evaluated t_w as the time during which the site's relative humidity (RH) exceeded some critical value (RH_c) with the dew point above 0°C plus the cumulative duration of rain events. The range of RH_c used was 75 to 95%, where 75% was found to be more appropriate for marine environments or locations where deicing salts are used. It was found that calculations for t_w using RH_c = 75% were approximately double those using RH_c = 90%; thus, Equation (2.3-4) accounts for the corrosive effect of chloride deposition by increasing t_w. When data on fence wire was excluded, Spence et al. (1992) found that the model accounted for 73% of the variability when estimating a set of field corrosion observations.

2.4. FIELD OBSERVATION OF GEOMETRY-DEPENDENT ATMOSPHERIC CORROSION RATE

A large body of literature exists on the field investigation of atmospheric corrosion. The major findings of a few such reports are summarized here.

Fuse et al. (2015) studied the state of corrosion in an actual transmission tower on the coast of Japan. Compared to skyward-facing surfaces and surfaces facing away from the sea, corrosion was found to be significant on ground- and sea-facing surfaces of members. Crevice corrosion may have attacked connections and bolts, but only steel angles are studied in the report. A final relevant observation by Fuse et al. (2015) is that greater corrosion was observed on samples taken from

greater heights in the tower; the stated assumption was that this was due to greater wind speed and thus higher chloride deposition with elevation.

Jeffrey and Melchers (2008) conducted a corrosion trial for mild steel coupons (100 x 50 x 3 mm) and strips (6000 x 50 x 3 mm) at a highly corrosive site 200 m from the ocean in Newcastle, Australia. The aim of the project was to study the effect of different factors on corrosion, including direction of exposure (N, S, E, or W), inclination, target size, and elevation. The backs of some coupons were coated with rubber with the goal of preventing corrosion on that face; after three years, these were the only coupons remaining, as the rest had completely oxidized. An unexpected result of the study is that for vertically-oriented coupons exposed in the cardinal directions, the north and west-facing specimens experienced 30-40% more corrosion than south and east-facing coupons; since the ocean is southeast of the site and the prevailing wind is from the southeast, it was expected that the south and east-facing coupons would corrode the most. In a separate set of samples, an octagonal drum was used to expose samples northward, skyward, southward, groundward, and at 45° between these directions. The south-groundward angle was found to experience the most corrosion after 3 years, while the directions immediately adjacent (southward and groundward) experienced the least. It was concluded that no single factor could explain the corrosion rates observed in the inclination study; humidity, rainfall, time-of-wetness, chloride deposition, wind speed, wind direction, solar radiation, and reflected radiation were noted as factors, and further study was recommended to better understand their contribution to corrosion rate. The coupons were observed to corrode two to three times more than the steel strips. Finally, corrosion was observed to generally increase slightly with height up to 2 m and then remain constant or drop at heights up to 6 m (the greatest height tested).

Rajagopalan et al. (1971) conducted a corrosivity study on 6 x 4 x 1/16 in metal panels at a tropical location on the southeast coast of India. Different factors studied included type of metal (including zinc and mild steel), distance from the ocean, elevation, angle of exposure, and shelter from sun and rain vs. exposed conditions. Fully exposed samples had higher corrosion rates than sheltered samples, and skyward-facing samples corroded faster than samples facing the ground. Vertically oriented samples were observed to corrode faster than horizontal samples while samples at ground level corroded faster than samples elevated 45 ft.

Further survey of field corrosion studies leads to the conclusion that the positional atmospheric corrosion behavior of metals is highly site- and condition-specific and can be difficult to predict in advance.

CHAPTER 3

DEVELOPMENT OF TOWER CORROSION MODEL

3.1. INTRODUCTION

This chapter introduces two new methods for modeling corrosion in galvanized steel lattice transmission towers. The first, described in section 3.2, applies only to the galvanized zinc coating of each tower member and is based on the work of Spence et al. (1992).

Using the model of Spence et al. (1992) requires adopting a specific set of assumptions about the corrosivity pattern at a particular site. As seen in sections 2.3 and 2.4, however, corrosion behavior can vary widely; thus, the second corrosion formulation (section 3.3) is proposed as a more general approach to capture corrosivity trends not covered by the assumptions of Spence et al. (1992).

3.2. DEPOSITION MODEL FOR ZINC COATING CORROSION

Steel lattice towers are comprised mainly of bars and angle members. For predicting the corrosion effect of airflow perpendicular to bars, the application of the Spence et al. (1992) model is somewhat straightforward. Spence et al. (1992) measured corrosion by taking mass loss for the entire sample, so no distinction is made between material loss on panel edges vs. loss on the faces; for now the same approach is taken here, and the bar edge and face are assumed to corrode at the same rate. Similarly, for Equation (2.3-6), Spence et al. (1992) makes no distinction between airflow on horizontal and vertically-oriented steel panels; the same assumption is made here, so airflow perpendicular on both the tall and short bar surfaces is treated as laminar, as shown below. Note that the model in section 3.3 will treat these as distinct cases.

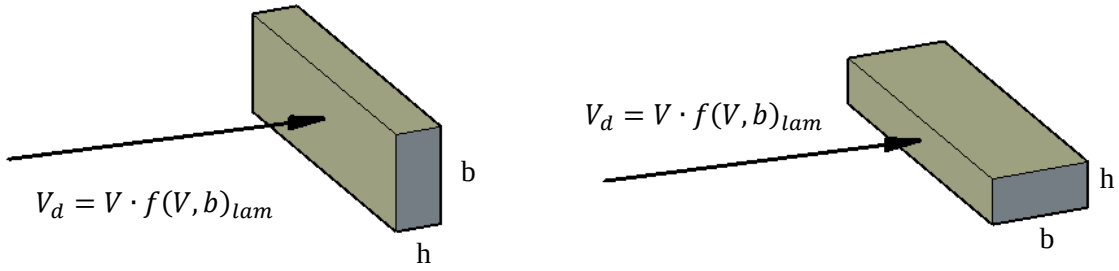

Figure 3.2-1. Both bar orientations in relation to perpendicular wind are treated as laminar flow of the same magnitude by Spence et al. (1992). The black arrow indicates wind direction.

For airflow parallel to a bar's length, however, it is assumed here that the flow will become turbulent and thus Equation (2.3-8) is adopted. The same assumption is made for flow parallel to an angle member's length:

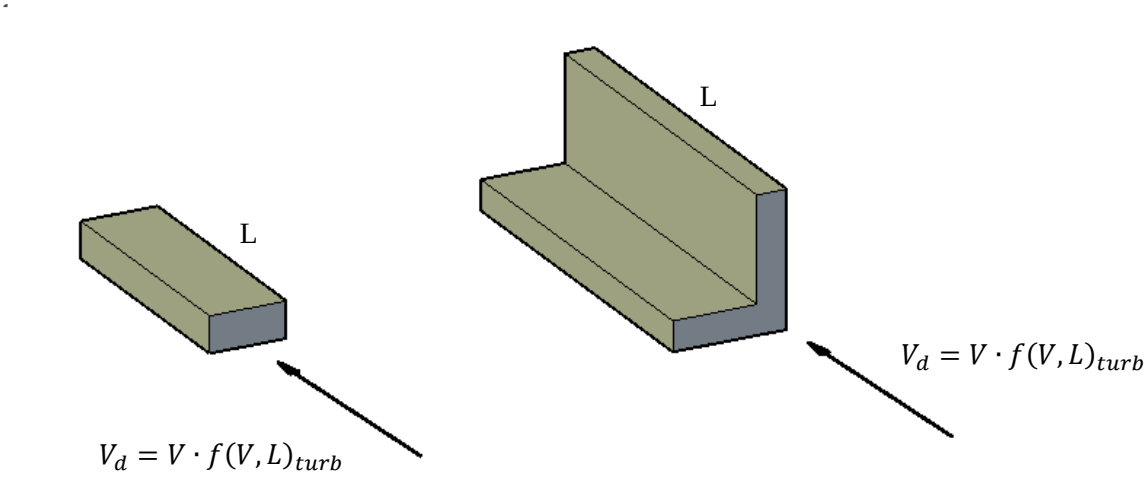

Figure 3.2-2. Wind parallel to length of bars and angles is assumed to be turbulent.

Since only flat surfaces and wires are treated by Spence et al. (1992), additional assumptions must be made for airflow perpendicular to the width of steel angle members. For steel

bars, a uniform corrosion rate on all four surfaces of each bar was assumed, following the example of Spence et al. (1992). For angles, however, each of the six cross-sectional surfaces (t_2, t_3, t_{2back}, t_{3back}, t_f, t_w – see Figure 3.2-3 below) is assumed to corrode at a distinct rate, matching the field observations of those such as Fuse et al. (2015) where corrosion rates were found to depend on the orientation of each angle member surface.

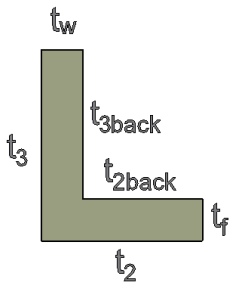

Figure 3.2-3. Adopted labels for the six surfaces of a simplified model of a steel angle. It should be noted that while t_f and t_w are in reality slightly curved, they are approximated to be flat in this work for simplicity.

Each surface is modeled to experience a distinct deposition velocity and thus corrosion rate. Four orientations of a steel angle relative to perpendicular, horizontal wind attack then need to be considered for modeling a transmission tower: θ = 0°, 90°, 180°, and 270°:

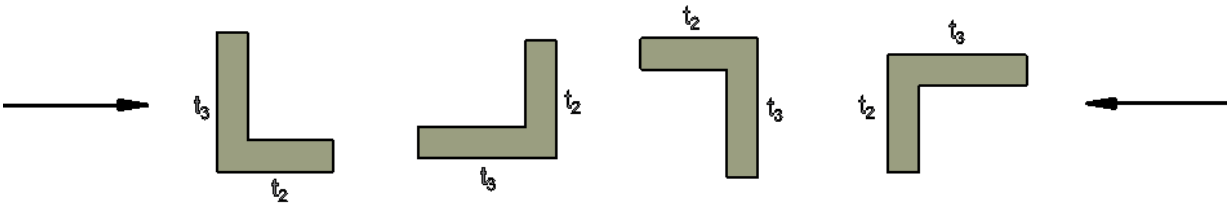

Figure 3.2-4. Four base case orientations to be considered for steel angles: θ = 0°, 90°, 180°, and 270° respectively. Wind must be considered as impinging from either horizontal direction as shown.

To illustrate the application of these assumptions, calculations for deposition velocity on the six surfaces in the 0° orientation are now described for wind coming from the "right." For t_f, t_{2back}, and t_2, airflow is assumed to remain laminar, and thus the small panel solution for deposition velocity in Table 2.3-1 is applied:

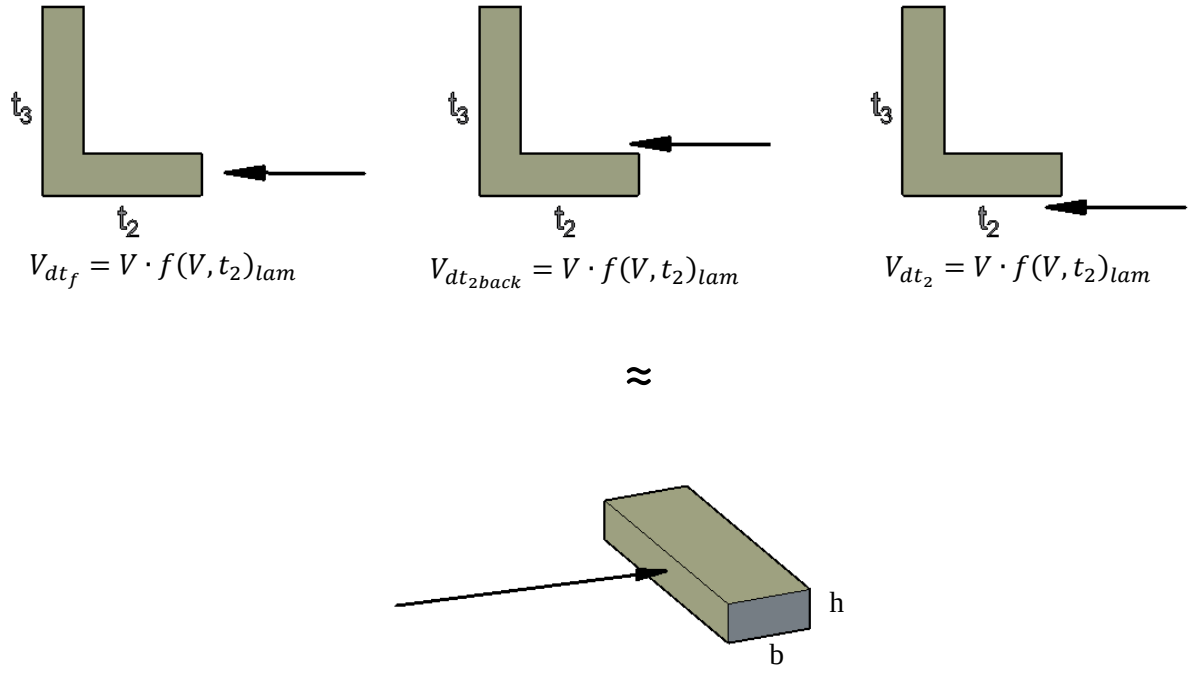

Figure 3.2-5. The deposition velocity on t_f, t_{2back}, and t_2 is assumed to equal the base case of deposition onto a flat panel with a characteristic length of $x = t_2$.

Note that for t_{2back}, in reality some turbulence would be expected as airflow approaches t_{3back}:

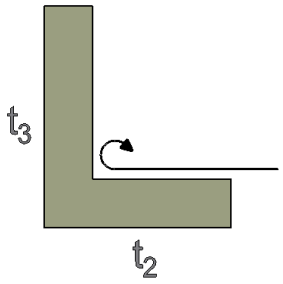

Figure 3.2-6. Turbulence as airflow approaches t_{3back}.

As before, turbulence is assumed to inhibit particle deposition. As seen in Figure 3.2-5, the turbulence effect depicted in Figure 3.2-6 was therefore accounted for by using $f(V, t_2)_{lam}$ instead of $f(V, t_{2back})_{lam}$ when calculating $V_{dt_{2back}}$, as the slightly larger length of t_2 acts to decrease $f(V, x)$.

The other three surfaces are expected to experience additional turbulent effects as airflow has already traveled across other surfaces before reaching them. In these cases (t_{3back}, t_w, and t_3), deposition velocity is calculated by assuming the average of the impinging wind paths on that surface, shown in Figures 3.2-6, 3.2-7, and 3.2-8 respectively.

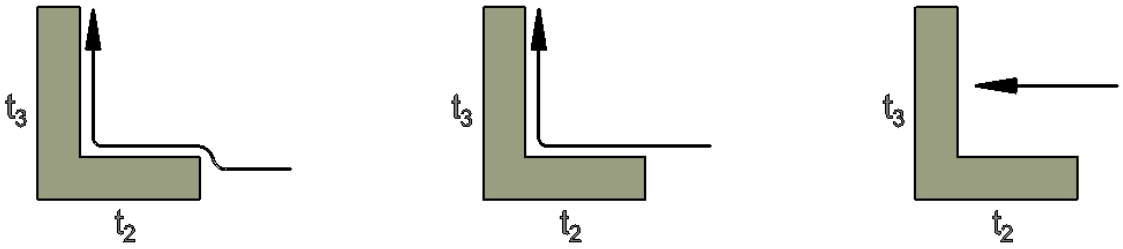

$$V_{dt_{3back}} = \frac{V}{3} \cdot \Big(f\big(V, 0.5 \cdot t_f + t_{2back} + t_{3back}\big)_{turb} + f(V, t_{2back} + t_{3back})_{turb} + f(V, t_{3back})_{lam} \Big)$$

Figure 3.2-6. The deposition velocity on t_{3back} is assumed to equal the average of three different flow paths – two turbulent and one laminar.

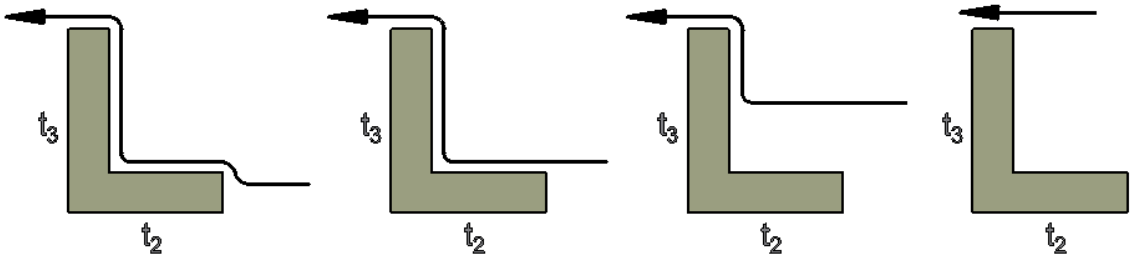

$$V_{dt_w} = \frac{V}{4} \cdot \Big(f\big(V, 0.5 \cdot t_f + t_{2back} + t_{3back} + t_w\big)_{turb} + f(V, t_{2back} + t_{3back} + t_w)_{turb} + 2 \cdot f(V, t_{3back})_{lam} \Big)$$

Figure 3.2-7. The deposition velocity on t_w is assumed to equal the average of four different flow paths – two turbulent and two laminar equal to the base case of characteristic length x = t_{3back}.

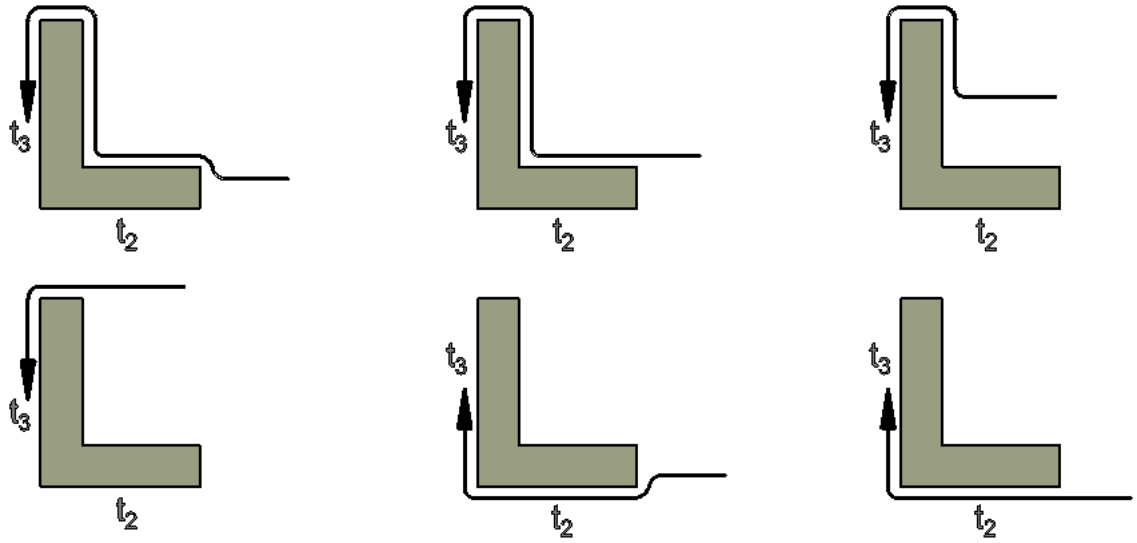

$$V_{dt_w} = \frac{V}{6} \cdot \Big(f\big(V, 0.5 \cdot t_f + t_{2back} + t_{3back} + t_w + t_3\big)_{turb} + f(V, t_{2back} + t_{3back} + t_w + t_3)_{turb} + 2 \cdot f(V, t_{3back})_{lam} + f\big(V, 0.5 \cdot t_f + t_2 + t_3\big)_{turb} + f(V, t_2 + t_3)_{turb} \Big)$$

Figure 3.2-8. The deposition velocity on t_3 for the 0° orientation with wind coming from the right is assumed to equal the average of six different flow paths – four turbulent and two laminar.

As noted, in this model the result of the assumed turbulent effects is a decrease in deposition rate. Comparing V_{dt_3} to V_{dt_f}, for example – assuming the 0° orientation, a 3.5 m/s wind from the right, and a 1.75" x 1.25" x 0.125" angle (t_2 x t_3 x t_f = t_w) – V_{dt_f} exceeds V_{dt_3} by 0.577 cm/s (2.282 vs. 1.705 cm/s). This mimics the shielding effect on leeward/inside surfaces observed by Fuse et al. (2015) and others. A similar effect results from the calculations for the other four member orientations (90°, 180°, and 270°) and wind directions ("left" and "right"). For the 90° orientation with wind from the right, for example, a shielding effect is observed on t_{3back}.

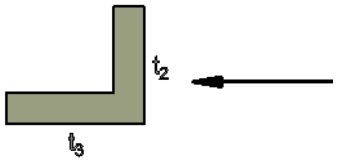

Figure 3.2-9. Bold wind attack on surface t_2 in the 90° position.

In this case, with the same angle and wind speed as above, V_{dt_3} = 2.031 cm/s and $V_{dt_{3back}}$ = 1.137 cm/s. Similarly, for the 180° position and wind from the right, t_{2back} experiences a shielding effect:

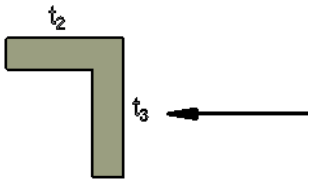

Figure 3.2-10. Bold wind attack on surface t_3 in the 180° position.

In the case depicted in Figure 3.2-10, $V_{dt_{2back}}$ = 1.140 cm/s and V_{dt_2} = 1.812 cm/s – opposite the case shown in Figure 3.2-9, where the groundward surface experienced greater

corrosion. The ratio between skyward and groundward corrosion in this model is therefore dependent on orientation and wind attack and changes for each member.

Since members in a transmission tower do not all sit horizontally in the cardinal directions, deposition velocity for wind attacking a member at an angle is interpolated between the perpendicular and parallel cases. For a bar sitting at 45° to wind attack in the horizontal plane, for example, $V_d = \frac{V}{2}(f(V,b)_{lam} + f(V,L)_{turb})$. This interpolation is extended for members in any position in three-dimensional space.

Further, the fact that wind speed increases with elevation is used to account for the increase in corrosion rate with elevation observed by Fuse et al. (2015), Jeffrey and Melchers (2008), and others. Dyrbye and Hansen (1997) present the following equation for increasing wind speed with height:

$$V(z) = V(z_{ref}) \cdot \left(\frac{z}{z_{ref}}\right)^{\alpha} \tag{3.3-9}$$

where z is the elevation of interest, z_{ref} is the elevation at which wind speed has been reported (typically 10 m), and α is a roughness parameter depending on the surrounding landscape. Typical values of α are presented in Table 3.2-1:

Table 3.2-1. Wind speed as a function of height: Dyrbye and Hansen (1997)

Terrain category		α
I	Rough, open sea, lakes with at least 5 km fetch upwind and smooth flat country without obstacles	0.12
II	Farmland with boundary hedges, occasional small farm structures, houses or trees	0.16
III	Suburban or industrial areas and permanent forests	0.22
IV	Urban areas in which at least 15% of the surface is covered by buildings with an average height exceeding 15 m	0.30

The term $\exp(-21.34 + 3651/T)$ in Equation (2.3-4) represents the contribution to zinc corrosion of atmospheric CO_2 and was derived by Spence et al. (1992) for the concentration of 345 ppm (typical for the 1980s, the time of the field corrosion studies referenced in that work). A brief reference to possibly increasing zinc corrosion with CO_2 concentration is given by Spence et al. (1992) based on thermodynamic relationships, but a direction relation is not presented. This positive relationship is confirmed by a laboratory study by Falk et al. (1998) where zinc corrosion was observed to increase between 350 and 1000 ppm. Further research is needed to confirm this corrosion increase, but based on the thermodynamic relationships presented by Spence and Haynie (1990), the effect of rising CO_2 on zinc corrosion is considered in this corrosion model. This is done through the following simple relationship, shown here for the first time. Spence and Haynie (1990) show that the solubility of zinc ions in a solution of carbon dioxide and water is

$$Zn^{2+} = [k(CO_2)^{1.6}/4]^{1/3} \tag{3.2-10}$$

where Zn^{2+} is zinc ion concentration in mol/L, k is an equilibrium constant in mol/L, and CO_2 is carbon dioxide atmospheric concentration in atm. k is shown to be independent of CO_2 and $Zn^{2+}(345\text{ ppm})$ has already been shown to equal $\exp(-21.34 + 3651/T)$; therefore a simple division with Equation 3.2-10 results in

$$Zn^{2+}(CO_2, T) = \left(\frac{CO_2}{345}\right)^{8/15} \exp(-21.34 + 3651/T) \tag{3.2-11}$$

with CO_2 in ppm. Substituting Equation (3.2-11) for $\exp(-21.34 + 3651/T)$ in Equation (2.3-4) allows a potential change in zinc corrosion due to rising atmospheric CO2 concentration to be accounted for.

Equation (2.3-4) is linear in time and was derived based on exposure periods as low as 2 years. For longer exposures, however, corrosion depth generally follows the general form of

$$D = r_{corr} t^b \tag{3.2-12}$$

where r_{corr} is the corrosion depth in the first year, t is time in years, and b is a constant usually less than 1 (ISO 9224, 2012). Additionally, for times greater than approximately 20 years, corrosion is generally observed to become linear as the rate of metal loss approaches the loss from the layer of corrosion products on the surface (ISO 9224, 2012). Thus, per ISO 9224 (2012):

$$D(t > 20) = r_{corr}[20^b + b(20^{b-1})(t - 20)] \tag{3.2-13}$$

By defining r_{corr} as the result of Equation 2.3-4 and b as defined in ISO 9224 (0.813 ± 0.03), these time-dependent functions are adopted.

When the zinc coating has been depleted, the underlying steel begins to corrode. The model described in section 3.3 is then applied.

3.3. FIELD OBSERVATION MODEL FOR ZINC AND STEEL CORROSION

The model for zinc corrosion presented in section 3.2 makes a specific set of assumptions about corrosion behavior in a transmission tower – specifically, that corrosion decreases as surface from horizontal and member size increases, and corrosion increases with elevation and greater exposure to wind. As seen in sections 2.3 and 2.4, depending on local conditions, all of these assumptions may be wrong for a transmission tower, however. For either the zinc coating or the underlying steel, the model proposed in this section allows more flexibility in specifying the nature of corrosion attack on a tower.

For each of the four member orientations, (0°, 90°, 180°, and 270°), an exposure matrix is created based on the corrosion behavior expected or observed at a particular site. For angles, this takes the following form:

Table 3.3-2. Example exposure matrix for steel angle member for each of the cardinal directions, skyward, and upward.

		Exposure direction					
		N	S	E	W	Up	Down
Surface	t_2	0.8	1.2	1.33	0.67	0.9	1.3
	t_3	0.8	1.21	1.33	0.67	0.9	1.3
	t_{2back}	0.9	1.1	1.35	0.7	0.8	1.33
	t_{3back}	0.9	1.1	1.36	0.7	0.8	1.33
	t_w	0.95	1.25	1.37	0.9	0.95	1.37
	t_f	0.95	1.25	1.37	0.92	0.95	1.37

Each entry acts as a multiplication factor E_r for some base corrosion rate C. For surface t_w oriented skyward, for example, the expected corrosion rate would be $0.95C$. Thus Table 3.3-2 represents a site where greater corrosion is expected on south, east, and ground-facing surfaces, and the smallest surfaces (t_w and t_f) experience the greatest corrosion rate. For a bar member:

Table 3.3-3. Example exposure matrix for bar

		Exposure direction					
		N	S	E	W	Up	Down
Surface	b	0.8	1.2	1.35	0.67	0.9	1.3
	h	0.95	1.25	1.37	0.9	0.95	1.37

Note that since bars are symmetrical, only two rows are needed to fully define the expected corrosion behavior in the given directions. Each of the four surfaces (both b's and both h's) experience a distinct corrosion rate, however, given that each faces a different direction. This is a departure from the model presented in section 3.2, where all four surfaces were assumed to corrode at the same rate.

For members sitting at an angle, interpolation between the exposure matrix values is carried out as before in three-dimensional space. Additionally, two more exposure factors, E_{elev} and E_{size}, are defined in the model. E_{elev} is a function of the member's elevation, allowing the variation of corrosion of height to be specified. Likewise, E_{size} allows size effects to be defined (distinguishing between a 1.75" x 1.25" angle and a 1.75" x 1.75" angle, for example).

Using Equations 3.2-12 and 3.2-13 to define time-varying corrosion, it is recognized that the b term may also change based on exposure (Benarie and Lipfert, 1986). Factors E_b are thus defined by exposure tables as well.

For this model, the base corrosion rate C for zinc and/or steel is defined as that given in ISO 9223 (2012), which depends on temperature, relative humidity, SO_2 deposition, and Cl^- deposition. The b term for zinc has been noted in section 3.2; per ISO 9224, b for steel is 0.523 ± 0.026. The total attack for a given surface is then

$$D = E_r E_{elev} E_{size} C t^{E_b b} \tag{3.3-14}$$

Similarly, Equation 3.2-13 is applied for times greater than 20 years.

CHAPTER 4

SIMULATION RESULTS AND ANALYSIS

The corrosion behavior and hurricane performance of a tower near the coast of Texas is studied in this chapter. The base OpenSEES finite element model was built by Mohammadi Darestani et al. (2019) and therefore accounts for buckling effects, joint slippage and failure, and construction material and geometry uncertainty. Their OpenSEES model has been adapted here to allow each cross section of the 576 tower members to be individually defined and therefore corrode at different rates. The assumed orientation of the tower with transverse wind loading for pushover analysis is shown in Figure 4-1 below.

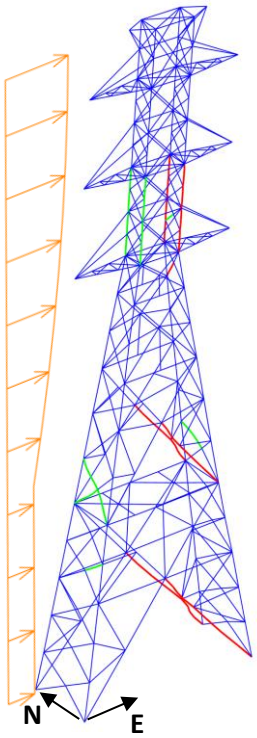

Figure 4-1. Orientation of the assumed tower with transverse loading. The tower shown has failed in a particular simulation with red members indicating failure in compression and green indicating failure in tension. No joint failure is observed in this case.

Environmental parameters for the corrosion attack are gathered from Spence et al. (1992) and other sources. The MATLAB code used to define corrosion attack allows all environmental parameters (wind speed, SO_2, etc.) to be specified on an annual basis. The historical and projected change in CO_2 shown by Marchal et al. (2011) was therefore adopted for the following simulations.

Member coating thickness is first estimated by taking the minimum required values from ASTM A123 (2017). A zinc coating of 100 μm is given to a bar with a minimum dimension between 0.25" and 0.65", for example, while a bar with a minimum dimension of between 0.1875" and 0.25" is given a zinc coating of 75 μm.

The model presented in section 3.3 for both zinc and steel (henceforth referred to as the Exposure or ISO model) is used to simulate the corrosion attack from 0 to 20 years of service, 2020 to 2039. To simulate the maximum expected attack, b has been set at two standard deviations above the typical values (ISO 9224), and worst-case environmental parameters have been selected.

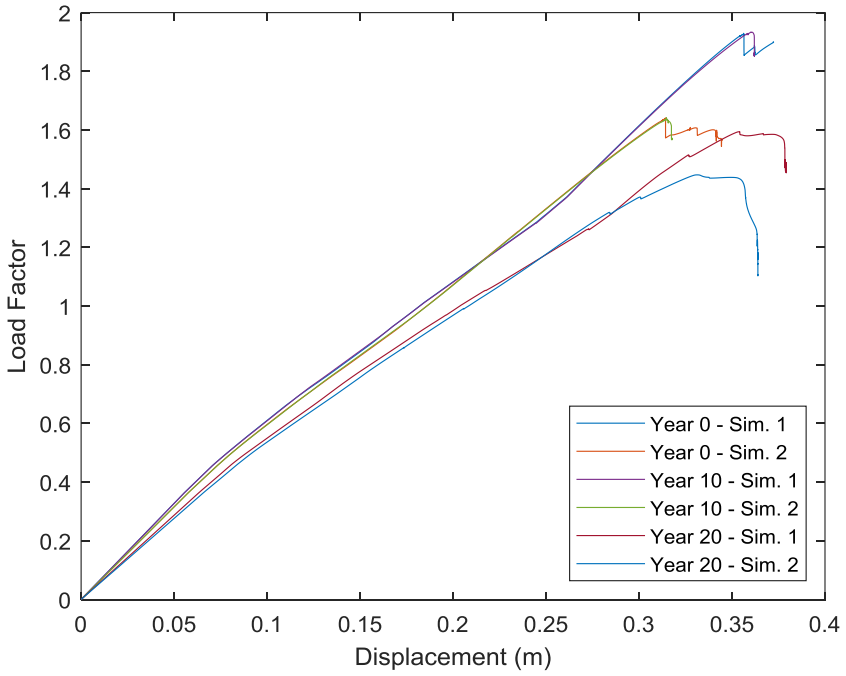

Figure 4-2. Pushover analysis with a Category 3 hurricane. A Load Factor of 1 corresponds to the tower meeting its design wind speed of 130 mph. Displacement is measured at a node at the top of the tower.

"Sim. 1" and "Sim. 2" represent two different realizations of material and geometric uncertainty as shown in Mohammadi Darestani et al. (2019). It can be seen that thanks to the protection of the galvanized coating, after 10 years, corrosion has had little effect on the structural performance of the tower; the first instance of steel substrate corrosion only occurs in 2026. By 2039, however, corrosion has caused a significant reduction in load bearing capacity.

To study the effect of uniform corrosion as opposed to the geometry-dependent models presented here, the steel corrosion depths from the Year 20 - Sim. 1 corrosion attack above are weighted by each affected surface area and averaged to generate a uniform corrosion rate for the entire tower, resulting in 775 μm steel loss per surface. This uniform attack is then simulated with the same realization parameters as before:

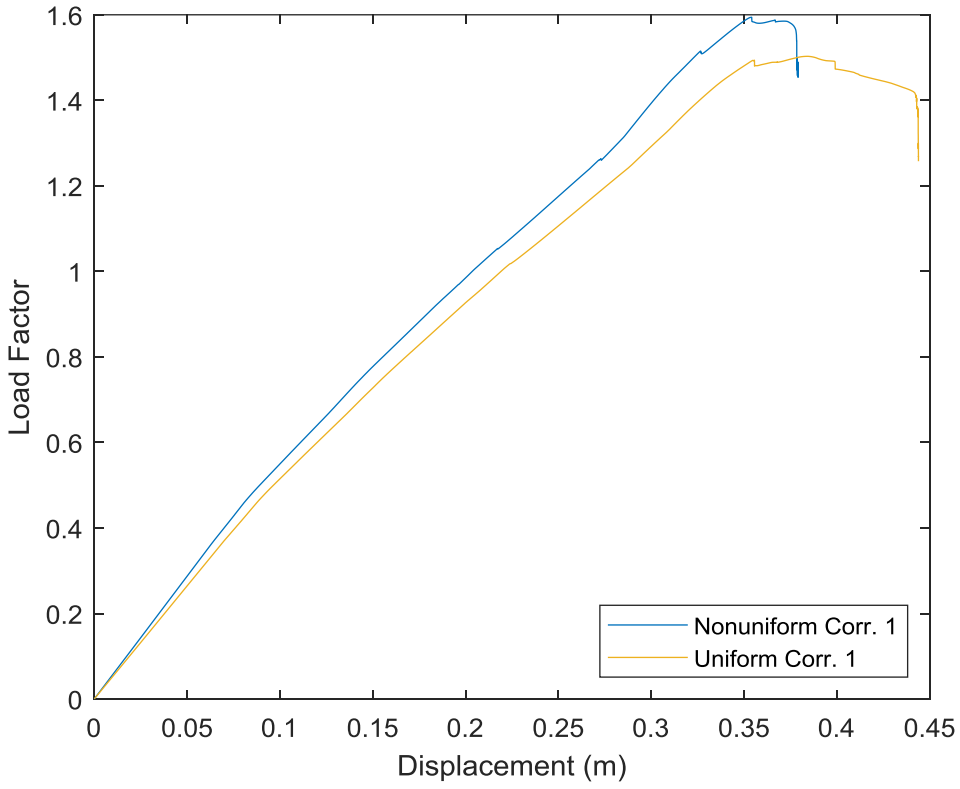

Figure 4-3. Transverse loading of uniform vs. nonuniform tower corrosion.

As seen in Figure 4-3, the uniform attack results in lower load-bearing capacity. This is likely due to the fact that in the nonuniform case, the biggest tower members have greater coating thicknesses and also experience less corrosion attack due to E_{size}. In the uniform corrosion simulation, however, initial coating thickness is ignored and the largest, normally protected members experience the same steel corrosion depth as all other members.

The constant coating thickness used by Salazar and Mendoza (2008) is now adopted: 85 μm. Using the same procedure as above, for a 10-year exposure the nonuniform corrosion by the ISO/Exposure model is averaged and applied to the whole tower to obtain a uniform corrosion attack. The result of the uniform attack pushover analysis is plotted here against the nonuniform:

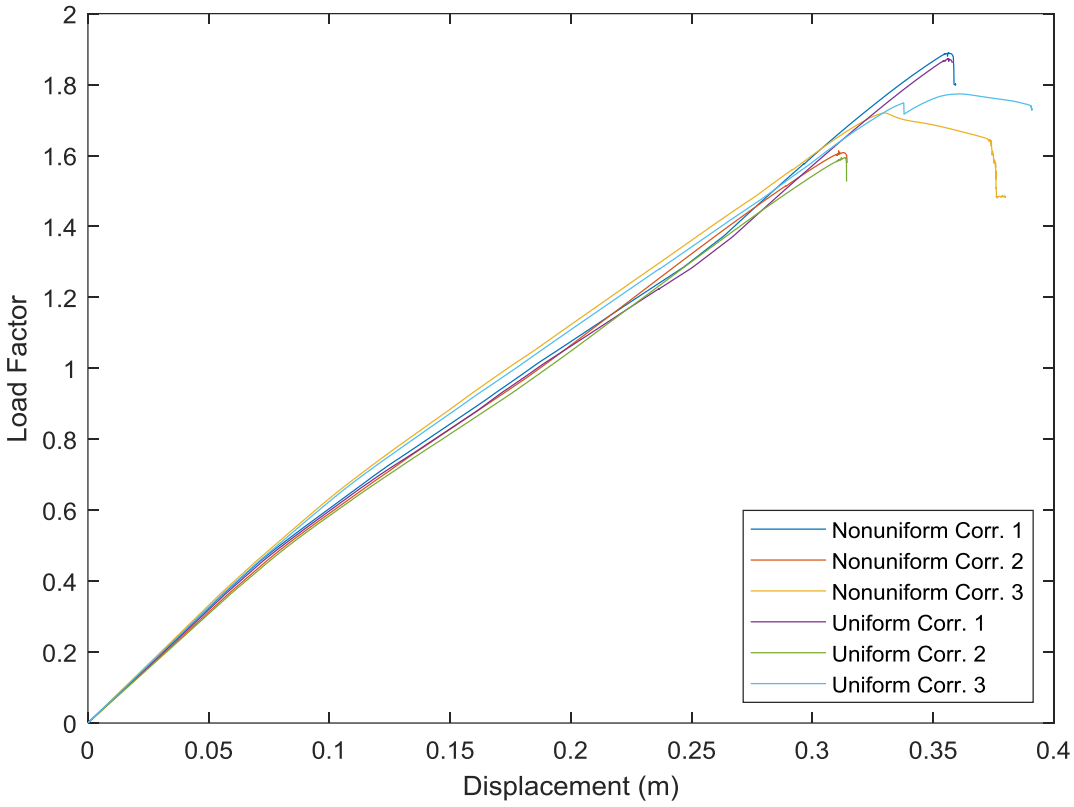

Figure 4-4. Uniform coating thickness of 85 μm, uniform vs. nonuniform tower corrosion.

As seen in Figure 4-4, two of the realizations (1 and 2) result in a slightly lower load factor for the uniform attack, while the third realization results in the nonuniform attack experiencing a comparatively much greater reduction in capacity.

Rodger et al. (2017) studied the coating thicknesses C_t of freshly galvanized members from a galvanizing plant in Brisbane, Australia and found the following relationship:

$$C_t = \begin{cases} 45s - 34 \text{ for } s \leq 6 \text{ mm} \\ 236 \text{ µm for } s > 6 \text{ mm} \end{cases} \quad (4\text{-}15)$$

where s is the member's minimum section thickness. This may be the most realistic representation of tower coating thickness presented thus far. For a 10 year service using the Exposure/ISO nonuniform attack model, the three coating thickness estimations are plotted against each other for comparison:

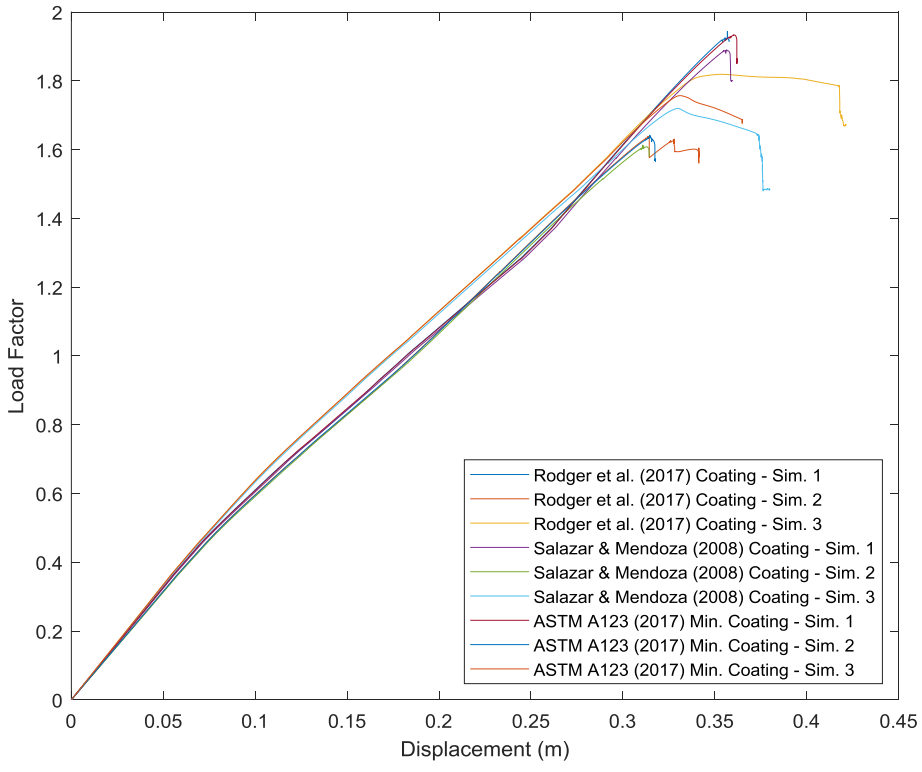

Figure 4-5. 3 representations of coating thickness on a galvanized steel tower

As expected, the uniform 85 μm coating of Salazar and Mendoza (2008) has the worst behavior, as it results in the thinnest overall coating for all members. The coating thicknesses of the ASTM 123 minimum and the Rodger et al. study have comparable performance, except for one realization in which the Rodger et al. coating greatly outperforms the rest.

Only the Exposure model has been used thus far, with exposure matrices specifying the greatest attack on surfaces facing the east, slightly lower attack on surfaces facing south, and less attack for northward and westward surfaces. The Spence et al. (1992) corrosion model is now simulated for comparison. For input to the Spence et al. model, the average prevailing wind directions were accessed from the Weather Spark (2016) website for Houston; the site reports that wind is most often from the south for 8.9 months annually, from the east 3.6 weeks, and from the north for 2.3 months. $8.9/12 = 0.74$, $(3.6/4)/12 = 0.07$, and $2.3/12 = 0.19$ were therefore used in the model to scale the zinc corrosion effects from those three directions. The tower thus experiences the greatest zinc corrosion on surfaces facing south, and less zinc corrosion on surfaces facing other directions. The same exposure matrices as described above are used for steel corrosion, however, so steel exposed facing east still corrodes the fastest. Other parameters of the Spence et al. model were adjusted to achieve nearly the same surface area-averaged steel loss as the Exposure model for a 10 year attack, resulting in an average of 131.619 μm loss on the Exposure model and 131.618 μm on the Spence et al. model.

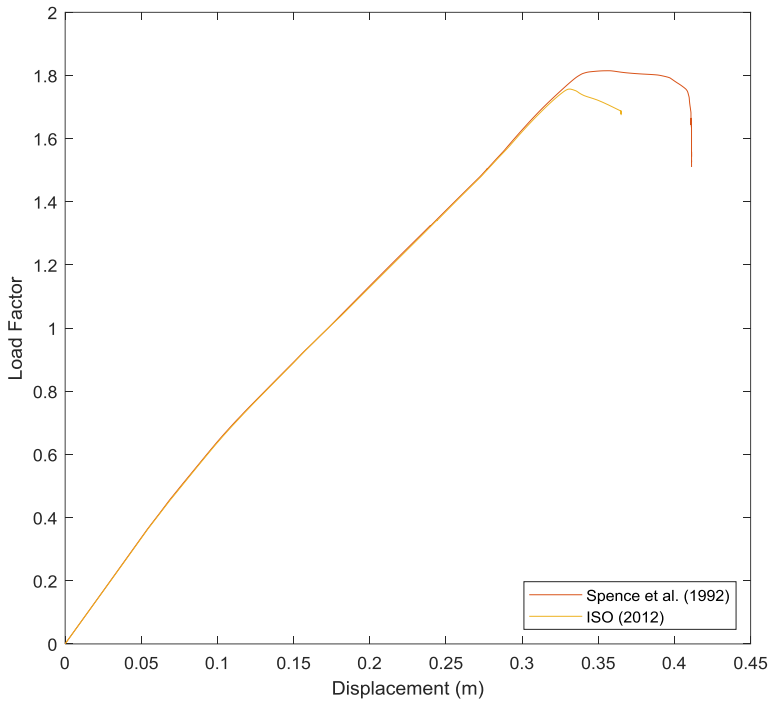

Figure 4-6. Transverse loading (from the west) on the Spence et al. corrosion model (primarily southward corrosion for zinc, eastward for steel) and the ISO Exposure model (primarily eastward corrosion for zinc and steel)

The Exposure/ISO model (eastward corrosion) has markedly less load bearing capacity in this comparison, and the 0.001 μm greater steel loss is unlikely to be the cause. Further study is needed for these directional effects; while overall steel loss was surface area averaged, zinc coating loss was not.

CONCLUSION

This study found that the simulated structural performance of galvanized steel lattice transmission towers changes based on assumptions of uniform vs. nonuniform corrosion, uniform vs. nonuniform coating thickness, and the nature of the nonuniform corrosion pattern. Further research is needed to fully understand the nature of these effects on tower performance, perhaps including using as input an actual tower's corrosion damage on each member rather than exposure matrices. Additionally, more data may be needed to confirm the relationship between atmospheric CO_2 concentration and zinc corrosion rate shown in section 3.2. Future study may also wish to perform CFD simulations or actual wind tunnel trials on structural bars and steel angles to test the flow assumptions made in section 3.2.

REFERENCES

ASTM A123 / A123M-17, Standard Specification for Zinc (Hot-Dip Galvanized) Coatings on Iron and Steel Products, ASTM International, West Conshohocken, PA, 2017, www.astm.org

Benarie M. and Lipfert F. (1986). A general corrosion function in terms of atmospheric pollutant concentrations and rain pH. *Atmospheric Environment*. 20(10):1947-1958

Campbell R. (2012). Weather-Related Power Outages and Electric System Resiliency: Congressional Research Service.

Cole I. and Paterson D. (2013). Holistic model for atmospheric corrosion Part 5 – Factors controlling deposition of salt aerosol on candles, plates and buildings. *Corrosion Processes and Corrosion Control.* 39(2):125-130

Downey J. (2018). Duke Energy: Up to 3M customers in the Carolinas could lose power due to Hurricane Florence. Charlotte Business Journal.

Falk T., Svensson J., and Johansson L. (1998). The Influence of CO2 and NaCl on the Atmospheric Corrosion of Zinc: A Laboratory Study. *The Electrochemical Society*. 145(9):2993-2999.

Fuse N., Naganuma A., Fukuchi T., Hori Y., Mizuno M., and Fukunaga K. Underfilm corrosion of transmission tower cross-arms service-used in a pacific coast area. *Corrosion*. 2015;71(11):1387-1397. doi: http://dx.doi.org.proxy.lib.ohio-state.edu/10.5006/1736.

Hidy G. (1984). "Aerosols – An Industrial and Environmental Science". Academic Press, Inc.

ISO 9223. (2012). Corrosion of metals and alloys – Corrosivity of atmospheres – Classification, determination and estimation. International Organization for Standardization, Geneva, Switzerland.

ISO 9224. (2012). Corrosion of metals and alloys – Corrosivity of atmospheres – Guiding values for the corrosivity categories. International Organization for Standardization, Geneva, Switzerland.

ISO 9225. (2012). Corrosion of metals and alloys – Corrosivity of atmospheres – Measurement of environmental parameters affecting corrosivity of atmospheres. International Organization for Standardization, Geneva, Switzerland.

Jeffrey R. and Melchers R. (2008). Three year observations of corrosion losses for steels at a severe marine atmospheric site. 48th Annual Conference of the Australasian Corrosion Association: Corrosion and Prevention 2008. 715-726.

Klassen R. and Roberge P. (2000). Modeling the Effects of Local Topography on Atmospheric Corrosivity. NACE 2000, Paper No. 272, Orlando, Florida.

Klassen R., Hinton B., and Roberge P. (2000). Aerosol Model Aids Interpretation of Corrosivity Measurements in a Tropical Region of Australia. *Marine Corrosion in Tropical Environments, ASTM STP 1399*, Dean S., Delgadillo G., and Bushman J., Eds. American Society for Testing and Materials, West Conshohocken, PA, 2000.

Lipfert W. and Wyzga E. (1982). Application of a Theory for Economic Assessment of Corrosion Damage. ACS Symposium Serious; American Chemical Society. 411-430. 411-430. 10.1021/bk-1986-0318.ch029.

Marchal V., Dellink R., van Vuuren D., Clapp C., Château J., Lanzi E., Magné B., van Vliet J. (2011). OECD Environmental Outlook to 2050, Climate Change Chapter.

Yousef Mohammadi Darestani, Abdollah Shafieezadeh & Kyunghwa Cha (2019): Effect of modelling complexities on extreme wind hazard performance of steel lattice transmission towers, Structure and Infrastructure Engineering, DOI: 10.1080/15732479.2019.1673783

Niu H., Li X., and Zhang W. (2018). Capacity assessment of existing corroded overhead power line structures subjected to synoptic winds. *Wind and Structures*. 27(5):325-336. https://doi.org/10.12989/was.2018.27.5.325

K. S. Rajagopalan, P. Annamalai, M. Sundaram, C. Rajagopal and V. Chandrasekaran (1971). Atmospheric Corrosion of Metals at Mandapam Camp, India. *British Corrosion Journal*,

Rodger J, Bartlett S, and Atrens A. (2017). Corrosion of the galvanizing of galvanized-steel electricity transmission towers. *Materials and Corrosion*. 2017;(8):902. doi:10.1002/maco.201609351.

Salazar J. and Mendoza J. (2008). Life Prediction of Electrical Power Transmission Towers. *2008 Proceedings of the 9th Biennial Conference on Engineering Systems Design and Analysis*. 2. 10.1115/ESDA2008-59490.

Spence J. and Haynie F. (1990). ASTM 1000. ASTM, Philadelphia, PA. p. 208.

Spence J., Haynie F., Lipfert F., Cramer S., and McDonald L. (1992). Atmospheric Corrosion Model for Galvanized Steel Structures. *Corrosion*.

Weather Spark. (2016). "Average Weather in Houston." Cedar Lake Ventures, Inc. Accessed from https://weatherspark.com/y/9247/Average-Weather-in-Houston-Texas-United-States-Year-Round